PHOTONICS Research

0.33 mJ, 104.3 W dissipative soliton resonance based on a figure-of-9 double-clad Tm-doped oscillator and an all-fiber MOPA system

Zhijian Zheng,[1] Deqin Ouyang,[2] Xikui Ren,[1] Jinzhang Wang,[1] Jihong Pei,[3] and Shuangchen Ruan[1,*]

[1]Shenzhen Key Laboratory of Laser Engineering, Key Laboratory of Advanced Optical Precision Manufacturing Technology of Guangdong Higher Education Institutes, Guangdong Provincial Key Laboratory of Micro/Nano Optomechatronics Engineering, Shenzhen University, Shenzhen 518060, China
[2]Sino-German College of Intelligent Manufacturing, Shenzhen Technology University, Shenzhen 518118, China
[3]Key Laboratory of ATR National Defense Science and Technology, College of Information Engineering, Shenzhen University, Shenzhen 518060, China
*Corresponding author: scruan@szu.edu.cn

Received 31 October 2018; revised 17 February 2019; accepted 8 March 2019; posted 8 March 2019 (Doc. ID 349745); published 15 April 2019

We demonstrate, for the first time, to the best of our knowledge, an all-fiber figure-of-9 double-clad Tm-doped fiber laser operating in the dissipative soliton resonance (DSR) regime. Stable mode-locked rectangular pulses are obtained by using the nonlinear amplifying loop mirror (NALM) technique. A long spool of high-nonlinearity fiber (HNLF) and a segment of SMF-28 fiber are used to enhance the nonlinearity of the NALM loop and to obtain a large all-anomalous regime. Output power and pulse energy are further boosted by using a three-stage master oscillator power amplifier (MOPA) system. At the maximum pump power, average output power of up to 104.3 W with record pulse energy of 0.33 mJ is achieved with a 2 μm DSR-based MOPA system.

https://doi.org/10.1364/PRJ.7.000513

1. INTRODUCTION

Mode-locked pulsed fiber lasers have become a hot topic in scientific research because of their significant application value in many fields, such as material processing [1,2], medicine [3,4], remote sensing [5,6], and nonlinear optics [7]. A mode-locked pulsed fiber laser can generate a conventional negative-dispersion soliton, a stretched pulse, a self-similar pulse, and a dissipative soliton under different intracavity dispersion characteristics. In addition to a dissipative soliton, the energy of other pulses is often limited to 0.1–13.8 nJ [8–11]. A dissipative soliton can withstand higher nonlinear effects, which can effectively avoid pulse splitting, thus achieving a high-energy pulse output.

In 2008, Akhmediev *et al.* theoretically predicted the generation of extremely high energy directly from a mode-locked laser oscillator based on the cubic-quintic Ginzburg–Landau equation [12]. Subsequently, Chang *et al.* proposed the concept of dissipative soliton resonance (DSR), which indicates that the energy of a soliton can increase indefinitely under suitable conditions [13]. They also proposed that DSR can be produced in either the normal dispersion or the anomalous dispersion region [14–16]. Due to its superiority in obtaining large pulse energy and a tunable pulse width, more and more researchers have been conducting a lot of experimental research on DSR. In a 1 μm band, Liu *et al.* first observed the DSR operation in an Yb-doped ring cavity fiber laser with the nonlinear polarization rotation (NPR) technique [17]. The duration of the rectangular pulses increased with rise of pump power. At maximum output power of 12.65 mW, the corresponding pulse energy was 3.24 nJ. Then, Li *et al.* reported similar experimental results and increased the pulse energy to 54.6 nJ with a high optical-to-optical conversion efficiency of 46% [18]. Cai *et al.* obtained a high peak power of 1.1 kW and pulse energy of 160 nJ in an Yb-doped figure-of-8 laser, which was operating in the DSR regime [19]. In a 1.5 μm band, Wu *et al.* observed an Er-doped DSR mode-locked fiber laser in an all-normal-dispersion regime for the first time [20]. Mode-locked square-profile dissipative solitons were realized by the NPR technique in a ring cavity. The pulse energy of the square-profile dissipative solitons increased to 281.2 nJ without pulse breaking or distortion. Later, Li *et al.* first reported high-energy rectangular DSR in an anomalous dispersion regime [21]. A rectangular pulse with pulse energy as high as 715 nJ was realized in a long ring cavity. Wang *et al.* demonstrated DSR in a figure-of-8 laser, which was mode-locked by using the nonlinear amplifying loop mirror (NALM) technique [22]. Their experimental results revealed that the cause of the DSR pulse is independent of the specific mode-locking technique. At present, it is

reported that the average output power and pulse energy of a DSR mode-locked fiber laser can reach the W level and μJ level, respectively. Krzempek *et al.* focused on the DSR mode-locked double-clad Er:Yb fiber laser with different cavity structures such as figure-of-8 and figure-of-9, and scaled the DSR pulse energy to 1.011, 2.13, 2.3, and 6.5 μJ [23–26]. By employing two amplifiers in a figure-of-8 double-clad Er:Yb fiber laser, Semaan *et al.* demonstrated that a DSR mode-locked Er:Yb fiber laser has potential to generate pulse energy at the 10 μJ level [27]. It is worth noting that there are few reports on the 2-μm-band DSR mode-locked fiber laser, until Xu *et al.* demonstrated DSR mode-locked rectangular pulses of 19.51 nJ in a figure-of-8 Tm-doped fiber laser (TDFL) with net normal dispersion in 2015 [28]. In our previous report, we proposed and realized DSR operation in a figure-of-8 double-clad TDFL, and pulse energy was further scaled up to about the 100 μJ level [29]. Recently, figure-of-9 and σ-shaped oscillators were also designed to generate a DSR mode-locked single-clad TDFL, and energy of up to 400 nJ could be extracted directly from the oscillator [30,31].

As can be seen from above, DSR mode-locking is considered an efficient way to generate nanosecond large-energy pulses besides *Q*-switching and gain-switching techniques. Oscillators such as a ring cavity, and figure-of-8, figure-of-9, and σ-shaped cavities are widely used in the generation of DSR. However, there is no report on a figure-of-9 double-clad TDFL working in the DSR regime, and there is still a lot of room for further improvement in pulse energy with this regime.

In this paper, we report, for the first time, on a figure-of-9 double-clad TDFL that is operating in the DSR regime. Furthermore, we use a multistage master oscillator power amplifier (MOPA) system to increase the average output power and pulse energy to up to 104.3 W and 0.33 mJ, respectively. These are, to the best of our knowledge, record power and pulse energy based on a 2-μm-band DSR-based MOPA system to date.

2. SCHEMATIC OF THE EXPERIMENTAL SETUP

A. Schematic of the Figure-of-9 DSR Laser Setup

The experimental setup of the proposed DSR laser is depicted in Fig. 1. The DSR laser oscillator is composed of a figure-of-9 configuration. A 793 nm multimode laser diode (LD) is utilized to pump the gain fiber with a maximum power of 12 W. The multimode pump light is coupled into the gain fiber via a $(2+1)\times 1$ pump combiner. The gain fiber is a 4-m-long double-clad Tm-doped fiber (TDF; Nufern, SM-TDF-10P/130-HE) with cladding absorption of 3.0 dB/m at 793 nm. The corresponding core/cladding diameter is 10/130 μm, respectively, with a group velocity dispersion (GVD) of −86 ps^2/km at 1.9 μm. A home-made cladding power stripper (CPS) is utilized to strip the unabsorbed pump light. Then, a 150-m-long high-nonlinearity fiber (HNLF; YOFC, NL-1550-ZERO) and a 470-m-long single-mode optical fiber (Corning, SMF-28) are used to enhance the nonlinearity of the NALM. The HNLF has a core/cladding diameter of 4/120 μm, respectively, a nonlinear coefficient of 11.68 $W^{-1}\cdot km^{-1}$, and a GVD of −20.31 ps^2/km at 1.9 μm. The SMF-28 has a core/cladding diameter of 9/125 μm, respectively, and dispersion of −71 ps^2/km at 1.9 μm. Although the core diameters of the HNLF and SMF-28 are quite different, these two fibers can be connected by fusion splicing and repeated arc discharges. The splice loss measured in the low-power regime is about 0.8 dB. For changing the polarization states of the cavity, a three-paddle fiber polarization controller (PC) is added into the fiber loop. The NALM is connected to a high-reflection mirror (HR) via a four-port fiber coupler, which exhibits a beam splitting ratio of 35:65. An isolator (ISO) is spliced to the output port of the DSR laser oscillator for preventing unwanted reflected light. Because the fibers used in the cavity are all anomalous at 1.9 μm, the DSR laser oscillator should operate in an all-anomalous regime. The total length of the cavity is about 629 m, corresponding to an estimated net anomalous dispersion of −37.12 ps^2.

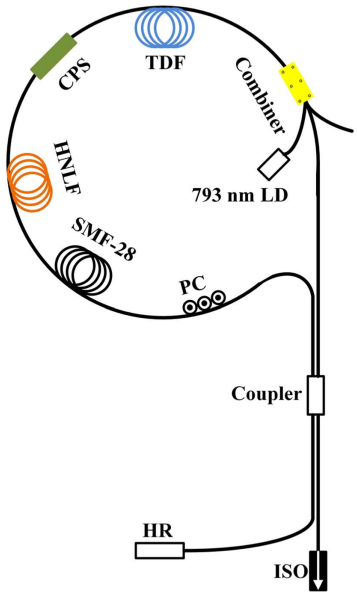

Fig. 1. Schematic of the proposed figure-of-9 DSR fiber laser.

B. Schematic of the Setup of the DSR-Based MOPA System

In order to obtain high power output, the DSR mode-locked signal is injected into a three-stage all-fiber MOPA system, as shown in Fig. 2. The first-stage amplifier (1st-Amp) and second-stage amplifier (2nd-Amp) have similar structures: both have a 16 W, 793 nm multimode LD and a 4-m-long TDF. The parameters of the TDF are the same as those in the figure-of-9 DSR laser. In the third-stage amplifier (3rd-Amp), large-mode-area (LMA) fibers are utilized for handling high-power operation. A high-power mode-field adaptor is utilized for mode-field matching between 2nd-Amp and 3rd-Amp. In

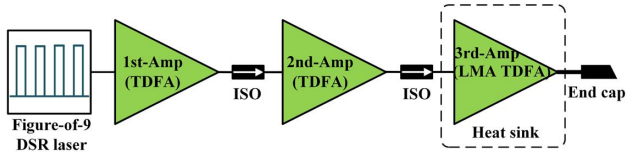

Fig. 2. Schematic of the high-power DSR-based all-fiber MOPA system.

3rd-Amp, two 120 W, 793 nm multimode LDs are used as the pump sources, which are connected to the gain fiber via a high-power-handling (2 + 1) × 1 pump combiner. The gain fiber is a 3-m-long LMA TDF (Nufern, LMA-TDF-25P/250-HE), which exhibits high cladding absorption of 9.5 dB/m at 793 nm, a core/cladding diameter of 25/250 μm, respectively, and a first cladding numerical aperture of 0.46. After the gain fiber, a high-power CPS is utilized to strip the unabsorbed pump light. Then an 8° polish with an anti-reflection coating end cap is used to deliver a high power output and avoid unwanted Fresnel reflection. For better thermal management, the whole 3rd-Amp is placed on a 5°C water-cooled heat sink.

In our experiment, the time-domain characteristic is measured with a 20 GS/s high-speed digital phosphor oscilloscope with a 1 GHz bandwidth (Tektronix, Inc., DPO 7104C), combined with a high-speed 2 μm photodetector with a bandwidth >12.5 GHz (Electro-Optics Technology, Inc., ET-5000); the rise/fall time is 28 ps. The output spectra are measured with an optical spectrum analyzer of 0.05 nm resolution (Yokogawa, Inc., AQ6375B). The frequency-domain characteristic is measured with a wide-frequency-span radio frequency (RF) spectrum analyzer (Agilent Technologies, Inc., E4407B), combined with the ET-5000 photodetector. The output power is measured with a high-sensitivity power meter (Coherent, Inc., Fieldmaster) and a high-power laser energy/power meter (Coherent, Inc., EPM2000).

3. EXPERIMENTAL RESULTS AND DISCUSSION

Figure 3 shows the output characteristics of the figure-of-9 DSR fiber laser. When the injected pump power reaches about 3.96 W, stable mode-locked rectangular pulses can be achieved. Figure 3(a) shows the pulse duration broadens from 12 to 262 ns with increase of pump power from 3.96 to 7 W; however, pulse profile and intensity remain nearly unchanged. The corresponding output spectra are shown in Fig. 3(b); with enhancement of pump power, not only does the spectral intensity increase, but also does the 3 dB spectral bandwidth, which increases from 12.3 to 16.6 nm. Meanwhile, the central wavelength is always located at ~1976 nm. We have further measured the RF spectrum characteristics of the figure-of-9 fiber laser when the pump power is 7.00 W, and corresponding pulse duration is 262 ns. Figure 3(c) shows the RF spectrum around the fundamental repetition rate with a 50 kHz span using a resolution bandwidth (RBW) of 1 Hz. The measured fundamental repetition rate, f_c, is 317.8 kHz and the signal-to-noise ratio is up to ~70 dB. Figure 3(d) shows a typical RF spectral distribution with a 20 MHz span using a 1 kHz RBW. It can be seen that the RF spectrum exhibits a periodic frequency modulation of $f_m = 3.81$ MHz, which is equivalent to the reciprocal of the corresponding pulse duration. Figure 3(e) plots the pulse parameters versus the average output power. It can be observed that the pulse energy generated and pulse duration change almost linearly with average output power. However, peak power remains at a relatively low level (0.26–0.49 W), mainly due to the peak power clamping effect. The obtained maximum average output power and pulse energy are 41.5 mW and 130.5 nJ, respectively. To test the long-term power stability of the figure-of-9 fiber laser, the output power is recorded continuously for 2 h at a pump power of 7.00 W. As shown in Fig. 3(f), the calculated mean output and the root-mean-square error (RMSE) are 41.3 and 0.26 mW, respectively. And the relative variation is only 0.63%, confirming that the figure-of-9 fiber laser is operating with high stability. The inset in Fig. 3(f) shows the autocorrelation trace obtained with an autocorrelator (APE, pulseCheck USB) for a wide scan range of 150 ps. It can confirm that the rectangular pulse envelopes did not contain any fine structures, and the figure-of-9 fiber laser is operating in the pure DSR mode-locking regime [25,32].

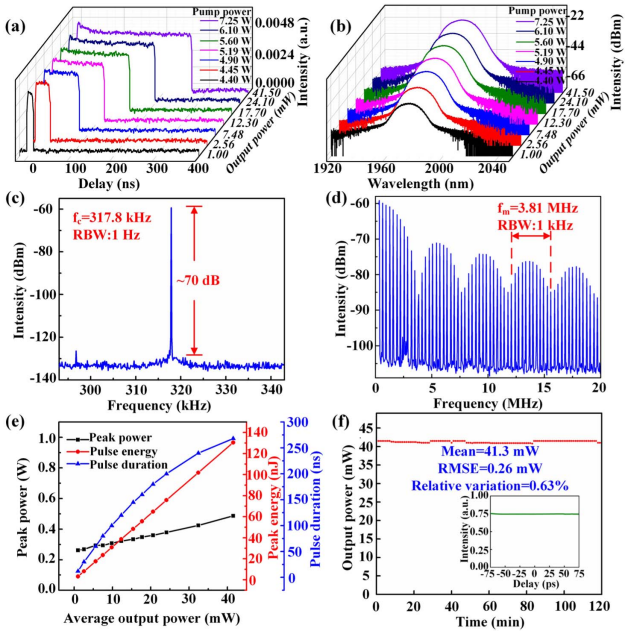

Fig. 3. Characteristics of the figure-of-9 double-clad DSR fiber laser. (a) Output pulse. (b) Output spectra. (c) RF spectrum at the fundamental repetition rate. (d) RF spectrum with a 20 MHz span. (e) Pulse parameters versus average output power. (f) Power stability. Inset: autocorrelation trace.

One of the noteworthy features of the rectangular pulses is that their pulse energy could be increased to a very high level without pulse distortion or pulse fission. In our experiment, we also boost the output power and pulse energy in a three-stage all-fiber MOPA system. High power output is obtained with the all-fiber MOPA system. For the amplifiers in the first two stages, maximum average output power of 4.04 W can be generated. Figure 4 shows that the intensity of the rectangular pulse is gradually strengthened with increase of the 2nd-Amp pump power from 6.78 to 15.40 W, although the pulse profile and duration remain nearly unchanged. So the pulse energy of the rectangular pulse can be further improved.

At 3rd-Amp, maximum pump power of up to ~210 W is launched into the LMA TDF and average output power at the 100 W level can be obtained. Figure 5(a) shows the average output power of the system versus the pump power injected into 3rd-Amp. The recorded maximum output power is 104.3 W, with a slope efficiency of ~50% and pulse energy of 0.33 mJ. The inset in Fig. 5(a) shows the maximum average output power. Figure 5(b) plots the output spectra at different

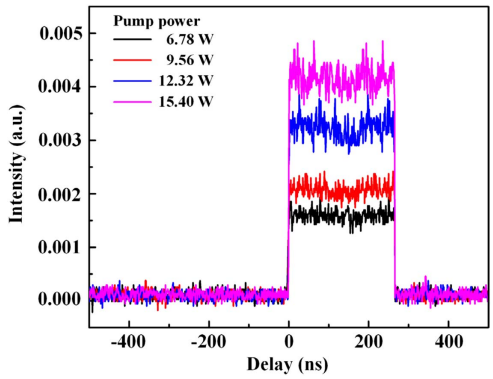

Fig. 4. Pulse intensity at different pump powers.

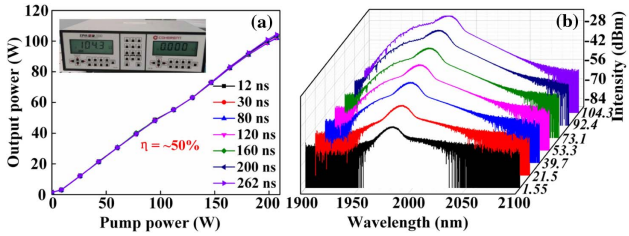

Fig. 5. Characteristics of the MOPA system. (a) Average output power of the system versus the pump power injected into 3rd-Amp. (b) Output spectra.

output powers. Due to the wide pulse duration, the peak power of the system is much lower than that in Ref. [29]; no obvious nonlinear effect is observed. The spectra obtained are slightly broadened, with maximum 3 dB spectral bandwidth of ~16.6 nm. As can be seen from Fig. 5, no power saturation and significant spectral broadening occur, so further improvement in output power is mainly limited by the available pump power.

4. CONCLUSIONS

In conclusion, a figure-of-9 double-clad TDFL that is working in the DSR regime and a DSR-based MOPA system are demonstrated. Rectangular pulses from the figure-of-9 double-clad TDFL are continuously tunable in the range of 12 to 262 ns and the maximum power/pulse energy obtained is 41.5 mW/130.5 nJ, respectively. The average output power and pulse energy are further scaled up to 104.3 W and 0.33 mJ, respectively, with the help of a multistage MOPA system. To the best of our knowledge, this is the first DSR operation of a figure-of-9 double-clad TDFL and the highest recorded power/pulse energy of a DSR-based MOPA system in the 2 μm band. The experiment proves that the DSR-based MOPA system has potential to be a candidate for generating high power/pulse energy in the nanosecond regime.

Funding. National Natural Science Foundation of China (NSFC) (11704260, 61575129, 61605122, 61775146); Natural Science Foundation of Guangdong Province (2016A030310049); Major Science and Technology Project of Guangdong Province (2014B010131006); Shenzhen Science and Technology Project (JCYJ20160427105041864, JSGG20160429114438287, KQJSCX20160226194031).

REFERENCES

1. R. Gattass and E. Mazur, "Femtosecond laser micromachining in transparent materials," Nat. Photonics **2**, 219–225 (2008).
2. K. Sugioka and Y. Cheng, "Ultrafast lasers—reliable tools for advanced materials processing," Light Sci. Appl. **3**, e149 (2014).
3. N. Fried and K. Murray, "High-power thulium fiber laser ablation of urinary tissues at 1.94 μm," J. Endourol. **19**, 25–31 (2005).
4. N. Fried, "Thulium fiber laser lithotripsy: an *in vitro* analysis of stone fragmentation using a modulated 110-watt thulium fiber laser at 1.94 μm," Lasers Surg. Med. **37**, 53–58 (2005).
5. P. Hajireza, W. Shi, K. Bell, R. Paproski, and R. Zemp, "Non-interferometric photoacoustic remote sensing microscopy," Light Sci. Appl. **6**, e16278 (2017).
6. S. Henderson and C. Hale, "Fast widely-tunable single-frequency 2-micron laser for remote-sensing applications," Proc. SPIE **10406**, 104060C (2017).
7. Z. Zheng, D. Ouyang, J. Zhao, M. Liu, S. Ruan, P. Yan, and J. Wang, "Scaling all-fiber mid-infrared supercontinuum up to 10 W-level based on thermal-spliced silica fiber and ZBLAN fiber," Photon. Res. **4**, 135–139 (2016).
8. J. Buckley, F. Wise, F. Ilday, and T. Sosnowski, "Femtosecond fiber lasers with pulse energies above 10 nJ," Opt. Lett. **30**, 1888–1890 (2005).
9. D. Dvoretskiy, V. Lazarev, V. Voropaev, Z. Rodnova, S. Sazonkin, S. Leonov, A. Pnev, V. Karasik, and A. Krylov, "High-energy, sub-100 fs, all-fiber stretched-pulse mode-locked Er-doped ring laser with a highly-nonlinear resonator," Opt. Express **23**, 33295–33300 (2015).
10. B. Nie, D. Pestov, F. Wise, and M. Dantus, "Generation of 42-fs and 10-nJ pulses from a fiber laser with self-similar evolution in the gain segment," Opt. Express **19**, 12074–12080 (2011).
11. J. Wang, Z. Jiang, H. Chen, J. Li, J. Yin, J. Wang, T. He, P. Yan, and S. Ruan, "High energy soliton pulse generation by a magnetron-sputtering-deposition-grown $MoTe_2$ saturable absorber," Photon. Res. **6**, 535–541 (2018).
12. N. Akhmediev, J. Soto-Crespo, and P. Grelu, "Roadmap to ultra-short record high-energy pulses out of laser oscillators," Phys. Lett. A **372**, 3124–3128 (2008).
13. W. Chang, A. Ankiewicz, J. Soto-Crespo, and N. Akhmediev, "Dissipative soliton resonances," Phys. Rev. A **78**, 23830 (2008).
14. W. Chang, A. Ankiewicz, J. Soto-Crespo, and N. Akhmediev, "Dissipative soliton resonances in laser models with parameter management," J. Opt. Soc. Am. B **25**, 1972–1977 (2008).
15. W. Chang, J. Soto-Crespo, A. Ankiewicz, and N. Akhmediev, "Dissipative soliton resonances in the anomalous dispersion regime," Phys. Rev. A **79**, 033840 (2009).
16. P. Grelu, W. Chang, A. Ankiewicz, J. Soto-Crespo, and N. Akhmediev, "Dissipative soliton resonance as a guideline for high-energy pulse laser oscillators," J. Opt. Soc. Am. B **27**, 2336–2341 (2010).
17. L. Liu, J. Liao, Q. Ning, W. Yu, A. Luo, S. Xu, Z. Luo, Z. Yang, and W. Xu, "Wave-breaking-free pulse in an all-fiber normal-dispersion Yb-doped fiber laser under dissipative soliton resonance condition," Opt. Express **21**, 27087–27092 (2013).
18. X. Li, S. Zhang, H. Zhang, M. Han, F. Wen, and Z. Yang, "Highly efficient rectangular pulse emission in a mode-locked fiber laser," IEEE Photon. Technol. Lett. **26**, 2082–2085 (2014).
19. J. Cai, S. Chen, and J. Hou, "1.1-kW Peak-power dissipative soliton resonance in a mode-locked Yb-fiber laser," IEEE Photon. Technol. Lett. **29**, 2191–2194 (2017).
20. X. Wu, D. Tang, H. Zhang, and L. Zhao, "Dissipative soliton resonance in an all-normal-dispersion erbium-doped fiber laser," Opt. Express **17**, 5580–5584 (2009).
21. X. Li, X. Liu, X. Hu, L. Wang, H. Lu, Y. Wang, and W. Zhao, "Long-cavity passively mode-locked fiber ring laser with high-energy

rectangular-shape pulses in anomalous dispersion regime," Opt. Lett. **35**, 3249–3251 (2010).
22. S. Wang, Q. Ning, A. Luo, Z. Lin, Z. Luo, and W. Xu, "Dissipative soliton resonance in a passively mode-locked figure-eight fiber laser," Opt. Express **21**, 2402–2407 (2013).
23. K. Krzempek, D. Tomaszewska, and K. Abramski, "Dissipative soliton resonance mode-locked all-polarization-maintaining double clad Er:Yb fiber laser," Opt. Express **25**, 24853–24860 (2017).
24. K. Krzempek, "Dissipative soliton resonances in all-fiber Er–Yb double clad figure-8 laser," Opt. Express **23**, 30651–30656 (2015).
25. K. Krzempek, J. Sotor, and K. Abramski, "Compact all-fiber figure-9 dissipative soliton resonance mode-locked double-clad Er:Yb laser," Opt. Lett. **41**, 4995–4998 (2016).
26. K. Krzempek and K. Abramski, "6.5 μJ pulses from a compact dissipative soliton resonance mode-locked erbium-ytterbium double clad (DC) laser," Laser Phys. Lett. **14**, 15101 (2017).
27. G. Semaan, F. Braham, J. Fourmont, M. Salhi, F. Bahloul, and F. Sanchez, "10 μJ dissipative soliton resonance square pulse in a dual amplifier figure-of-eight double-clad Er:Yb mode-locked fiber laser," Opt. Lett. **41**, 4767–4770 (2016).
28. Y. Xu, Y. Song, G. Du, P. Yan, C. Guo, G. Zhang, and S. Ruan, "Dissipative soliton resonance in a wavelength-tunable thulium-doped fiber laser with net-normal dispersion," IEEE Photon. J. **7**, 1502007 (2015).
29. J. Zhao, D. Ouyang, Z. Zheng, M. Liu, X. Ren, C. Li, S. Ruan, and W. Xie, "100 W dissipative soliton resonances from a thulium-doped double-clad all-fiber-format MOPA system," Opt. Express **24**, 12072–12081 (2016).
30. S. Kharitonov and C. Bres, "All-fiber dissipative soliton resonance mode-locked figure-9 thulium-doped fiber laser," in *Conference on Lasers and Electro-Optics Europe & European Quantum Electronics Conference (CLEO/Europe-EQEC)* (2017), p. 1.
31. T. Du, W. Li, Q. Ruan, K. Wang, N. Chen, and Z. Luo, "2 μm high-power dissipative soliton resonance in a compact σ-shaped Tm-doped double-clad fiber laser," Appl. Phys. Express **11**, 52701 (2018).
32. Y. Lyu, H. Shi, C. Wei, H. Li, J. Li, and Y. Liu, "Harmonic dissipative soliton resonance pulses in a fiber ring laser at different values of anomalous dispersion," Photon. Res. **5**, 612–616 (2017).